Unveiling the Intercompartmental Signaling Axis: Mitochondrial to ER Stress Response (MERSR) and its Impact on Proteostasis

Jeson J Li[1,2*], Nan Xin[1,2*], Chunxia Yang[1], Larrisa A Tavizon[2], Ruth Hong[3], Travis I Moore[1,2], Rebecca G Tharyan[4], Adam Antebi[4,5], Hyun-Eui Kim[1,2**]

1. Department of Integrative Biology and Pharmacology, McGovern Medical School, University of Texas Health Science Center at Houston, Houston, TX 77030, USA
2. The University of Texas MD Anderson Cancer Center UTHealth Houston Graduate School of Biomedical Sciences, Houston, TX 77030, USA
3. Geroge R. Brown School of Engineering, Rice University, Houston, TX 77030, USA
4. Max Planck Institute for Biology of Ageing, Joseph Stelzmann Str. 9b, 50931, Cologne, Germany
5. Cologne Excellence Cluster on Cellular Stress Responses in Aging-Associated Diseases (CECAD), University of Cologne, 50674, Cologne, Germany

* These authors contributed equally
**Correspondence: hyun-eui.kim@uth.tmc.edu

Abstract

Maintaining protein homeostasis is essential for cellular health. During times of protein stress, cells deploy unique defense mechanisms to achieve resolution. Our previous research uncovered a cross-compartmental Mitochondrial to Cytosolic Stress Response (MCSR), a unique stress response activated by the perturbation of mitochondrial proteostasis, which ultimately results in the improvement of proteostasis in the cytosol. Here, we found that this signaling axis also influences the unfolded protein response of the endoplasmic reticulum (UPR^{ER}), suggesting the presence of a Mitochondria to ER Stress Response (MERSR). During MERSR, the IRE1 branch of UPR^{ER} is inhibited, introducing a previously unknown regulatory component of MCSR. Moreover, proteostasis is enhanced through the upregulation of the PERK-eIF2a signaling pathway, increasing phosphorylation of eIF2a and improving the ER's capacity to manage greater proteostasis load. MERSR activation in both poly-glutamine (poly-Q) and amyloid-beta (Abeta) *C. elegans* disease models also leads to improvement in both aggregate burden and overall disease outcome. These findings shed light on the coordination between

the mitochondria and the ER in maintaining cellular proteostasis and provide further evidence for the importance of intercompartmental signaling.

Introduction

A cornerstone of maintaining physiological health is the ability of our cells to maintain protein homeostasis (proteostasis) during challenging times. Our cells have developed unique defense mechanisms to detect and resolve misfolded protein stress through the activation of complex signaling pathways. These pathways mediate the upregulation of chaperone proteins to aid in the proper folding of the misfolded proteins in addition to reducing protein load stress by shutting down the global protein translation[1]. Throughout evolution, our cells have evolved to compartmentalize, yielding functionally unique spaces to enhance the efficiency of biological functions[2]. With this also came the rise of compartmental stress responses within the ER, mitochondria, and cytosol. For quite some time, these cellular stress responses have been thought to be stand-alone systems, each encompassing its own unique set of regulatory elements and chaperone proteins. However, recent data from our lab suggests a cross regulatory network that mediates an intercompartment signaling axis.

Previously, we discovered that perturbation of the mitochondrial UPR (UPR^{MT}) through RNAi targeting mitochondrial HSP70 in *C. elegans* (HSP-6) resulted in an increase in the cytosolic heat shock response. This mitochondrial to cytosolic stress response (MCSR) improved cytosolic proteostasis in both *C. elegans* and human cell lines. Further evidence suggested that MCSR is regulated through the alteration of lipid metabolism, specifically ceramide and cardiolipin [3]. Although this was the first evidence of interaction between the mitochondria and the cytosol mediated through *hsp-6*, previous interactions between the mitochondria and ER have been described. Rizzuto et al. first characterized

the importance of mitochondria and ER contact sites (MERCS) in the regulation of calcium signaling[4]. MERCS has since been well studied and its role in multiple biological functions including Ca^{2+} signaling[5], lipid transport[6], mitochondria dynamics[7], and stress response[8] has been characterized. MERCS has also been implicated in an array of diseases including neurodegenerative disease[9] and cancer[10] and is currently being explored as a possible therapeutic target[11].

ER is the major site of secretory protein synthesis and the proper function of the UPR^{ER} is crucial to maintaining proper cellular function[12]. While *hsp-6* knockdown is able to induce MCSR and offers insight into the intercompartmental signaling axis between the mitochondria and cytosol, the question remains whether this axis exerts a dualistic influence over the ER. Indeed, our data suggests that the knockdown of *hsp-6* is able to improve UPR^{ER} by upregulating UPR^{ER} specific signaling pathways. Using animals harboring a transcriptional reporter of UPR^{ER} (*hsp-4*p::GFP), we observed a decrease in GFP fluorescence when treating the worms with tunicamycin followed by Mitochondria to ER Stress Response (MERSR) induction through *hsp-6* knockdown. Recent evidence suggests a regulatory roles of mitochondrial proteins on the UPR^{ER} and Integrated Stress Response (ISR) [13 14,15,16]; however, to our current knowledge, mitochondria induced UPR^{ER} signaling axis is undocumented and the influence of the mitochondria on the UPR^{ER} is currently a field that has not been well studied. Hence, more extensive work is needed to fully characterize this signaling axis.

We have previously shown that *hsp-6* knockdown reduces polyglutamine aggregates in the AM140 *C. elegans* strain that expresses polyglutamine repeats within body wall muscles[3]. We hypothesize that this decrease in aggregate abundance occurs partially through the activation of the UPR^{ER} signaling pathways. The activation of the UPR^{ER} signaling pathway increases the protein folding capacity of the

ER, which compensates for the increase in proteomic stress and ultimately helps to achieve ER stress resolution. When we perturbed the UPR^{ER} signaling pathway during *hsp-6* knockdown, we surprisingly found that the IRE1 branch of UPR^{ER} was inhibited. However, we found a significant increase in PERK-dependent eIF2 alpha phosphorylation, suggesting a decrease in global protein translation levels. Concomitantly, ER protein secretion capacity was also shown to be downregulated, suggesting a functional inhibition of the ER to further prevent the increase in misfolded proteins. Taken together, we can infer that MERSR is able to increase proteostasis through the upregulation of UPR^{ER} signaling pathways and is able to further reduces proteomic stress by suppressing ER protein secretion, ultimately leading to the increase in the capacity of the ER to combat increasing proteostasis.

Results

Tunicamycin induced ER stress is suppressed through the activation of MERSR

To determine the effect of MCSR on UPR^{ER}, we utilized a *C. elegans* reporter strain where a GFP tag has been fused to the promoter of a UPR^{ER} chaperone (SJ4005, *hsp-4p*::GFP). Tunicamycin treatment of the worms induced ER stress, resulting in GFP fluorescence that can be measured and quantified using fluorescent microscopy. SJ4005 worms were treated with tunicamycin during larval stage L4 followed by transfer onto RNAi plates containing *hsp-6* targeting RNAi sequences to induce MCSR. Loss of *hsp-6* resulted in a reduction of GFP fluorescence post-tunicamycin treatment when compared to empty vector control (Figure 1a). To determine if UPR^{ER} suppression was limited to tunicamycin or triggered by other ER stressors, we further targeted 2 distinct UPR^{ER} activators. 1) VCP is an AAATPase that among many other things, regulates ER-associated degradation (ERAD)[17]. The knockout of VCP is known to induce UPR^{ER} due to increased proteomic stress as a result of the increase in misfolded proteins[18]. 2) NFYB-1 is a histone-like transcription factor that regulates

mitochondrial function. Interestingly, it was found that NFYB-1 knockout exhibited cross-compartmental regulation and activation of UPR^{ER} [19]. Ultimately, *hsp-6* knockdown was able to reduce SJ4005 GFP fluorescence induced by loss of either NFYB-1 (Figure 1b) or VCP (Figure 1c), suggesting that downregulation of *hsp-6* is reflects an intrinsic mechanism that regulates an intercompartmental UPR signaling axis during times of stress. Interestingly, when we target transcription factors involved in the UPR^{MT} signaling pathway, such as *dve-1*, a similar reduction in UPR^{ER} reporter fluorescence level is observed (Figure S1a), suggesting that the reduced UPR^{ER} levels is a direct consequence of alterations that originate within the mitochondria. Post-developmental mitochondrial stress activated through *mrps-5*, *spg-7* and *cco-1* knockdown was unable to reduce UPR^{ER} signaling during tunicamycin treatment (Figure S1b). However, *cco-1* knockdown was able to reduce UPR^{ER} levels in *nfyb-1* mutants (Figure S1c), suggesting that post-developmental mitochondrial stress triggers a signaling cascade between the mitochondria and the ER. Collectively, our data suggests that *hsp-6* knockdown not only triggers MCSR, but also triggers a cross-compartmental signaling axis, activating a mitochondrial to ER Stress Response (MERSR).

Lipid metabolism mediates the ER suppression by *hsp-6* RNAi

We previously observed that the MCSR is mediated through altered lipid metabolism, in particular, the downregulation of ceramide and the upregulation of cardiolipins[3]. In *C. elegans*, *de novo* ceramide synthesis depends on the function of three separate ceramide synthase enzymes HYL-1, HYL-2 and LAGR-1, and the knockdown of these enzymes can alter the global sphingolipid landscape of the animals[20]. To investigate the possibility that sphingolipid metabolism also regulates MERSR, we targeted several critical enzymes in the *de novo* sphingolipid synthesis pathway in addition to cardiolipin synthase (*crls-1*) through RNAi. By inducing UPR^{ER} in SJ4005 reporter worms with *cdc-48*

mutant background followed by the perturbation of key sphingolipid synthesis enzymes through RNAi, we found that the knockdown of *hyl-1* exhibited a decrease in UPR^{ER} reporter intensity similar to that of *hsp-6* RNAi (Figure 2a). Other enzymatic targets within the *de novo* synthesis pathway however did not yield such results (Figure 2b). Conversely, when we knockdown cardiolipin synthase (*crls-1*), the inhibition of UPR^{ER} through *hsp-6* knockdown was negated (Figure 2c). These results suggest that not only do ceramide and cardiolipin mediate the stress signaling response between the mitochondria and the cytosol, but they also regulate the UPR^{ER} response initiated through the knockdown of *hsp-6.* The decrease in UPP^{ER} reporter signaling due to the knockdown of *hyl-1* could be the result of increased UPR^{ER} threshold caused by changes in ceramide levels, enhancing the capability of the cells to combat protein stress and therefore reducing GFP expression[21]. Furthermore, *nfyb-1* deleted mutant animals constitutively express higher levels of UPR^{ER} which could be reduced through the activation of MERSR (Figure 1b). Interestingly, the lipid profiles of these *nfyb-1* mutants exhibit a higher level of ceramide and lower levels of cardiolipin compared to their wild type counterparts[19]. The reduction in UPR^{ER} observed in these mutant animals through MERSR activation could be the result of decreased ceramide and increased cardiolipin content associated with MERSR.

MERSR is mediated through UPR^{ER} signaling pathway

UPR^{ER} signaling is mediated through three separate stress sensory pathways that work together to increase the capacity of the ER to combat proteomic stress[1]. During proteomic stress, ER signaling results in the upregulation of various chaperone proteins in order to aid in the proper folding and recycling of misfolded proteins[22]. In addition to increasing chaperone levels, another major compensatory mechanism of the ER is the PERK-eIF2a signaling pathway which attenuates global protein translation levels and reduces the total protein load of the ER[23]. To determine the effects of

MERSR on UPR^{ER} signaling pathways, we perturbed the UPR^{ER} signaling pathway during *hsp-6* knockdown and found that the double knockdown of *hsp-6* with *ire-1* or *xbp-1* resulted in the loss of MERSR activation (Figure 3a). Proper UPR^{ER} signaling is reliant on the dimer/oligomerization of IRE1, which differentially splices *xbp-1* mRNA to its active form *xbp-1*s. To investigate the impact of *hsp-6* knockdown on ectopic UPR^{ER} activation at two different points within the same pathway, we used 1) overexpression of IRE1, which would require proper IRE1 dimer/oligomerization, and 2) overexpression of *xbp-1*s (active form of *xbp-1*), allowing for the bypass of IRE1 dimer/oligomerization. Overexpression of IRE1 lacking the luminal domain (*ire-1* (344-967aa)) in the intestine induced UPR^{ER} signaling[24]. This induction was moderately reduced upon *hsp-6* knockdown. In contrast, *hsp-6* knockdown had no impact on *xbp-1*s overexpression-induced UPR^{ER} (Figure 3b), suggesting that the suppression of UPR^{ER} occurs upstream of *xbp-1*, possibly at a membrane level. One possibility is that *hsp-6* knockdown leads to an alteration in membrane fluidity, compromising the dimerization of the UPR^{ER} sensors. This is further corroborated by recent findings that the knockdown of ER-resident proteins alters the ER membrane lipid content, increasing mitochondria and ER contact through increasing membrane order[25]. Furthermore, alterations in lipid content within the ER membrane have been shown to induce UPR^{ER} in the absence of aberrant proteostasis[26], providing further evidence that membrane lipid content can directly influence the UPR^{ER} signaling pathways.

During times of proteomic stress, the activation of UPR^{ER} has also been shown to decrease global protein load through the phosphorylation of PERK-eIF2a signaling cascade[27]. Thus, we examined the levels of eIF2a phosphorylation during *hsp-6* knockdown. Along with PERK, we also targeted *gcn-2*, a PERK-independent eIF2a kinase activated primarily through amino acid starvation[28] and reactive oxygen species produced during mitochondrial stress[14]. Our data shows that *hsp-6* knockdown

enhances the phosphorylation level of eIF2a (Figure 3c), while the knockdown of *gcn-2* had no effect on either the induction or the suppression of UPR^{ER}. This suggests MERSR is able to increase the phosphorylation levels of eIF2a in a PERK-dependent manner. Moreover, when we performed double knockdown of *hsp-6* and *pek-1*, the inhibition of UPR^{ER} was no longer observed (Figure S2A), suggesting that the activation of MERSR is PERK dependent. Altogether, our data suggest that *hsp-6* knockdown enhances the UPR^{ER} through the increase of eIF2a phosphorylation via PERK signaling, reducing global protein translation levels to compensate for increasing ER stress.

Given that MERSR reduces global protein translation through the mediation of UPR^{ER} signaling, we further assessed the function of the UPR^{ER} by investigating its secretory capacity. In *C. elegans*, DAF-28 is one of 40 insulin-like peptides[29]. DAF28::GFP fusion protein is processed within the ER and secreted to the body cavities of the worms[30], eventually absorbed by the coelomocytes, a phagocytic and macrophage-like cells that engulf its surrounding materials for degradation[31]. GFP signal within the coelomocytes can be used as a readout to determine the ER secretion capacity of the cells[32]. We observed that the knockdown of *hsp-6* greatly reduced the GFP fluorescence within the coelomocytes (Figure 3d) to a level similar to that of ER dysfunction induced through the knockdown of *ire-1* and *xbp-1*. Western blots of daf-28 expression reporter worms GR1455 [*daf-28*p::GFP] and VB1605 [*daf-28*p::*daf-28*::GFP] further confirmed that the reduction observed in the coelomocytes during *hsp-6* RNAi was the result of decreased secretion rather than changes in the innate expression of *daf-28* (Figure S2b). This data suggests that the reduction in UPR^{ER} GFP reporter during MERSR, in addition to decreasing global translation through the upregulation of PERK-eIF2a signaling, also inhibits ER secretory functions. This reduction in ER protein secretion could serve as a compensatory mechanism during times of stress to further slow proteomic flux, allowing for ER stress resolution.

MERSR and ceramide reduction can benefit both ER and Cytosolic Stress-Related Neurodegenerative Diseases

Dysfunctional ER stress is a common phenotype in many neurodegenerative diseases, including Alzheimer's, Huntington's, and Parkinson's[33]. Early notions of ER stress denoted its function as deleterious[34]; however, recent studies have suggested that the response of UPR^{ER} in neurodegenerative diseases is highly dynamic[35]. Mild UPR^{ER} is upregulated during early stages of AD in order to resolve Abeta deposition, however, chronic Abeta burden as a result of advanced AD and constitutive UPR^{ER} activation triggers downstream apoptotic pathways, leading to cell death[36]. Abeta metabolism is a constant cycle, starting from the synthesis of Amyloid Precursor Protein (APP) in the ER, followed by the export to the Golgi and ultimately to the plasma membrane where it is cleaved by beta-secretase and gamma-secretase to form mature Abeta[37]. These findings naturally led us to explore the impact of MERSR on aggregate formation and clearance. We hypothesized that the decrease in ER secretory capacity during MERSR in combination with increased eIF2a phosphorylation would result in decreased Abeta burden and lead to improvements in overall disease state. First, we evaluated the physiological effects of Abeta burden by placing pan-neuronal AB1-42 worms under the effects of mild heat shock. When GRU102 (*myo-2*p::YFP + *unc-119*p::Abeta1-42) worms crossed with neuronal RNAi-sensitive strain (TU3401) are incubated at 25°C, the increased temperature accelerates the aggregate formation process, leading to rapid paralysis. However, the neuronal knockdown of *hsp-6* is able to delay the rate of paralysis, suggesting a decrease in Abeta aggregate burden (Figure 4a). Similarly, the knockdown of ceramide synthases (*hyl-1* and *hyl-2)* also improved the paralysis of neuronal Abeta-expressing animals. *hyl-1* knockdown also improved the

lifespan of these worms (Figure 4b), providing further evidence that lipid metabolism plays an integral role in the regulation of cross-compartmental stress response.

To determine whether MERSR also improves the proteostasis of animals expressing neuronal polyglutamine (poly-Q) repeats, we examined the AM101 (*F25B3.3p*::Q40::YFP) animals expressing neuronal poly-Q. Activation of MERSR through *hsp-6* knockdown, or the knockdown of *hyl-1* improved motility evident in the increase in the number of body bends of the worms (Figure 4c). Similarly, AM140 animals expressing poly-Q (Q35:YFP) in the body wall muscle showed decreased poly-Q aggregation (Figures 4d and e). Interestingly, this decrease in poly-Q aggregates required the presence of VCP (Cdc-48 in *C. elegans*), an essential component in ER-associated Degradation (ERAD) and the Ubiquitous Proteasome System (UPS). This data suggests that a properly functioning ERAD system is required for the proper cellular processing of these neurotoxic aggregates. Further evidence suggests that VCP is highly correlated with densely packed poly-Q aggregates, and upon MERSR activation, a portion of VCP becomes highly associated with loosely packed poly-Q aggregates. After immunostaining VCP and poly-Q aggregates in AM140 worms, the aggregates were categorized into loosely packed and densely packed by the staining intensity. In control animals, VCP predominantly colocalized with densely packed aggregates. However, in *hsp-6* RNAi treated animals, there was a notable increase in VCP colocalization with loosely packed aggregates (Figures 4f and g). These data suggest that the induction of MERSR is able to mobilize VCP to a subset of poly-Q aggregates. Although the downstream target of this VCP mobilization is unknown, given that the VCP function in aggregate handling is well characterized, we can postulate that VCP recruitment to the aggregates serves as a trigger for aggregate degradation through the UPS or macroautophagy.

These data suggest that MERSR activation and ceramide perturbation through *hyl-1* knockdown are able to improve the disease outcome of both cytosolic and ER associated neurotoxic aggregate worm lines. Taken together, our findings suggest that the increase in mitochondrial stress triggered through *hsp-6* knockout coordinates both cytosolic and ER stress responses, leading to enhanced cellular proteostasis through the upregulation of UPR^{ER} signaling pathways. Activation of MERSR in proteotoxicity models demonstrates its efficacy and inducibility in post-mitotic tissues such as neurons, further emphasizing the importance of this signaling pathway and the need for future research.

Discussion

Here we have identified an unexpected role of MCSR in promoting the balance of proteostasis by regulating the UPR^{ER} signaling pathways in *C. elegans*. Our study suggests that the knockdown of mitochondrial *hsp70* not only coordinates mitochondria to cytosolic stress response (3), but it also elicits an intercompartmental signaling axis between the mitochondria and the ER. Mitochondrial stress triggered by the knockdown of *hsp-6* results in decreased UPR^{ER} inducibility by multiple ER stress inducers, including tunicamycin, VCP knockout, and the loss of NFYB-1. The suppression of the IRE1 branch of the UPR^{ER} is mediated through perturbations of sphingolipid metabolism, suggesting the possibility of bioactive lipids serving as mediators along this intercompartmental signaling axis. Proper function of the UPR^{ER} is dependent on several signaling cascades. The PERK-eIF2a signaling cascade results in an increase in the phosphorylation of eIF2a, leading to a reduction in global protein translation levels. We have shown here that reduced UPR^{ER} inducibility is a direct result of increased PERK-dependent eIF2a phosphorylation in combination with decreased ER protein secretion. Interestingly, ERAD-related chaperone VCP was associated with loosely packed poly-Q aggregates in the muscle of AM140 animals when MERSR was activated. In these animals, MERSR reduced protein

aggregates in a VCP-dependent manner. Knocking down the *C. elegans* homologs of VCP abrogated the cytosolic proteostasis balance gained by MCSR (Figure 4f to g). It may suggest another scenario of cross-compartmental cooperation where ERAD-related VCP helps reduce the cytosolic protein aggregates. When VCP occupies cytosolic aggregates such as polyglutamine repeats, it may hinder ERAD activity and induce UPR^{ER}. This would be an intriguing question for the future of this research, to determine how cells meet the energy demand of mounting such stress responses when the mitochondria are under severe stress.

Mitochondria HSP70 (mtHSP70, mortalin, HSPA9, Grp75, HSP-6) is widely known for its beneficiary functions. It was first described as a substrate for protein translocation into the mitochondrial matrix[38]. However, as research on the subject has increased, the role of mortalin has begun to expand. Mortalin reduces the formation of reactive oxygen species and lipid peroxidation, protecting the mitochondria from oxidative stress[39]. In addition, mortalin exhibits protective properties against neurotoxicity in AD[40] and PD[41] through targeting of Abeta and alpha-synuclein, respectively. In light of this, an insightful review was recently published describing the link between mortalin and neurodegenerative disease[42]. Interestingly, in our study, the post-developmental knockdown of *hsp-6* in *C. elegans* conferred a protective phenotype against proteomic stress, suggesting a previously undiscovered role of mortalin. In support of our data, Honrath *et al*. also demonstrated a protective phenotype against glutamate induced oxidative cell death in Grp75 knockout HT22 cells[43]. However, this protection did not extend into drug-induced ER stress. This contradiction could be explained by the utilization of cancer cells in testing for ER stress protection. Cancer cells exhibit high levels of innate ER stress, and treatment with tunicamycin or thapsigargin may exacerbate ER stress and induce apoptotic signaling. In recent cancer research, mortalin has become a target for drug discovery due to its ability to bind P53 and

prevent its nuclear localization[44]. However, this colocalization is not observed in non-cancer cells[45], and the protective phenotype induced through *hsp-6* knockdown is still unknown. Despite this, given the significant changes in lipid metabolism, specifically cardiolipin and ceramide, it is likely that *hsp-6* knockdown-induced mitochondrial stress could result in the remodeling of the lipid composition within the mitochondrial membrane. Cardiolipin is a key regulator in the maintenance of mitochondrial membrane integrity and cristae morphology[46]. Proper cardiolipin metabolism is also responsible for mediating proper protein-protein and protein-membrane interactions[47] in addition to stabilizing the respiratory chain complex[48]. Although the displacement of cardiolipin and ceramide between the mitochondria and the ER during *hsp-6* knockdown remains undetermined, recent evidence revealed that *hsp-6* is inserted into the mitochondrial membrane and possesses an affinity for negatively charged phospholipids such as cardiolipin[49]. Indeed, cardiolipins are externalized during mitochondrial stress and serve as a signal for the induction signaling for mitophagic[50] and apoptotic[51] signaling; however, the exact mechanism of how cardiolipins regulate cross-compartmental signaling pathways will require further research.

Interestingly, ERAD-related chaperone VCP was associated with loosely packed poly-Q aggregates in the muscle of AM140 animals when MERSR was activated. In these animals, MERSR reduced protein aggregates in a VCP-dependent manner, and the knockdown of VCP resulted in the loss of proteostasis improvement. Although during ERAD, VCP is recruited to the surface of the ER by ubiquitin ligases to aid in the clearance of misfolded proteins[52], recent evidence shows strong support for the colocalization of VCP with neurotoxic aggregates[53]. The regulatory role of VCP in protein homeostasis occurs at multiple levels. During the initial process of aggregate formation, VCP regulates the UPS to detect and ultimately degrade misfolded proteins[54]. However, as aggregate burden

increases, VCP is able to regulate macroautophagy and aid in the removal of excess protein aggregates and damaged organelles to restore homeostasis[55]. In our study, we showed that VCP is essential in reducing poly-Q aggregates during MERSR; however, the downstream mechanisms of how aggregate clearance is achieved were beyond the scope of this paper. This does leave us with an exciting future research question of how mitochondrial stress regulates VCP activity to improve proteomic stress. Recent evidence has already shown VCP's involvement in the regulation of mitochondria and ER contact[56 57], further exacerbating the need for elucidation in this subject.

In conclusion, we have demonstrated for the first time, within our knowledge, the capabilities of a mitochondrial chaperone protein to regulate UPR^{ER} signaling through the perturbation of lipid metabolism. Current understanding of the relationship between the mitochondria and the ER is incomplete, although research on this subject has increased due to advances in biochemical and fluorescent microscopy. We know that mitochondria and the ER form contact sites in order to modulate membrane lipid composition and proper Ca^{2+} homeostasis. The question that remains is how *hsp-6* knockdown impacts mitochondria and ER contact. Although we did not explore this in our study, altered mitochondria and ER contact is seen in several tumor types as well as several neurodegenerative diseases, highlighting the importance of further research into this field.

Methods

Strains and Culture

AGD2797 (*unc-119*(*ed3*) III; uthSi71[*vha-6*p::mRuby::*xbp-1s*::*unc-54* 3'UTR, cb-*unc-119*(+)]) and AGD3156 (*unc-119*(*ed3*) III; uthSi65[*vha-6*p::ERss::mRuby::*ire-1a* (344-967aa)::*unc-54* 3'UTR cb-*unc-119*(+)] IV) were generous gifts from the Dillin lab (UC Berkeley).

SJ4005 (zcls4[*hsp-4*p::GFP]), CL2070 (dvIs70[*hsp-16.2*p::gfp]), AM140(rmIs132 [*unc-54*p::Q35::YFP]), AM101 (rmIs110 [F25B3.3p::Q40::YFP]), GRU102 (gnaIs2 [*myo-2*p::YFP + *unc-119*p::Abeta1-42]), TU3401(uIs69 [pCFJ90 (*myo-2*p::mCherry) + *unc-119*p::*sid-1*]), OK814 (*nfyb-1* (*cu13*)), N2 wild-type worms and the rest of the strains used were obtained from Caenorhabditis Genetic Center (CGC). All worm strains were grown at 20C using standard methods as described previously[58]. Nematode Growth Media (NGM) agar plates containing OP50 *E. coli* stain were used for normal growth, while HT115 bacteria was used for RNAi feeding. All RNAi clones were obtained from the Ahringer library[59].

RNAi Assays

Unless stated otherwise, HT115 containing RNAi sequences were cultured overnight in LB containing 100 ug/ml of carbenicillin. Cultures were then seeded onto NGM plates containing 1mM IPTG and stored in a blacked-out box to dry under dark conditions. The RNAi plates must be dried before use and long-term storage to ensure induction of T7 RNA polymerase activity. Worms were then transferred onto RNAi plates during their appropriate time points and grown at 20°C while remaining in the black box away from light. GFP reporter quantification was done by ImageJ. Worms were blindly picked under the LED dissecting microscope, then moved to the M805 Leica Fluorescent microscope to take the image. Then, individual worms were quantified with the ImageJ tools.

Western Blots

Post RNAi treated worms were washed with M9 buffer followed by lysis in RIPA buffer (50 mM Tris-HCl pH 7.5, 150 mM NaCl, 1% NP-40, 0.1% SDS, 2 mM EDTA, and 0.5% sodium deoxycholate) with protease inhibitor cocktail (Roche) at their appropriate time points. The homogenized lysate was then centrifuged at 13,000RPM for 10 minutes at 4°C. The supernatant was then transferred into a new 1.5mL tube to determine protein concentration using BCA assay (Invitrogen). 20-40 ug of protein was

loaded per lane in a pre-cast gel for SDS-PAGE (Bio-Rad). Gel was then transferred using the TurboBlot Transfer (Bio-Rad) followed by probing of phosphorylated eIF2a, a-tubulin, VCP and HSP-6. Quantification of bands was further carried out using ImageJ.

Immunohistochemistry

Worms were fixed by following the previously described Buoin's tube fixation method (Nenet et al., 1997) Nonet, M.L., Staunton, J.E., Kilgard, M.P., Fergestad, T., Hartwieg, E., Horvitz, H.R., Jorgensen, E.M., and Meyer, B.J. (1997). *Caenorhabditis elegans* mutant synapses exhibit impaired function and are partially depleted of vesicles. J. Neurosci. *17*, 8061–8073.

Briefly, 10 plates of worms with RNAi treatment were washed with M9 buffer and distilled water. Pelleted worms were fixed in Bouin's MB fix solution, followed by liquid nitrogen to crack the cuticles. Permeabilized worms were then washed with BTB solution and shaking incubated in BTB solution. BTB solution was replaced with BT solution before incubating with fresh antibody buffer. Antibodies were incubated as described in the antibody buffer. Images were taken using a Nikon A1R confocal laser scanning system equipped with a CIF Plan-Apo 100X objective (NA 1.49, Nikon) and ORCA-Flash 4.0 CMOS camera (Hamamatsu). Primary antibodies: VCP (Abcam), and YFP (Roche). Secondary antibodies: sheep 488 and mouse 647 (Invitrogen)

Paralysis Assay

Adult worms were synchronized using standard bleaching methods as described previously[60]. Worms were grown on standard NGM agar plates containing OP50 at 20C until day 1 adult. On day 1, 100 worms were transferred per RNAi condition onto NGM plates containing RNAi culture and transferred into the 25°C incubator. Worms were transferred onto fresh RNAi plates every other day, and paralysis of the worms was recorded every other days from day 1 to 5. Following day 5, the paralysis of the worms was recorded every day until all 100 worms were either dead or paralyzed. Worms that died

due to external circumstances and of natural causes were censored during data recording to maintain consistency throughout the experiment. Data was recorded and analyzed using Excel and Prism.

Body Bending Assay

Am101;Tu3401 worms were grown at 20°C on Nematode Growth Media (NGM) plates spotted with OP50 *E. coli*, then synchronized using the *C. elegans* standard bleaching method as mentioned previously[60]. On day 1 of adulthood, worms were transferred to NGM plates spotted with Empty Vector (EV), *hsp-6*, *hyl-1*, and *hyl-2* RNAi. They were incubated at 20°C (a typical incubation temperature for *C. elegans* growth) in the dark for the rest of the assay to prevent degradation of the IPTG that was inducing the RNAi. Worms were transferred to new RNAi plates every other day and progeny were removed on subsequent days as needed. Motility was measured on day 1 and day 5 of adult lifespan. To measure motility, worms were placed in a drop of M9 media and recorded for 30 seconds under a microscope. The number of body bends each worm performed within the 30 second timespan was manually counted and quantified with ImageJ.

DAF28::GFP Assay

Daf-28::GFP transgenic worms were synchronized using standardized *C. elegans* bleaching method and eggs were plated on OP50 plates at 20°C to allow for normal development. On day 1 of adulthood, the worms were treated with RNAi targeting *hsp-6*, *xbp-1*, *ire-1* and EV (control). Worms were transferred to new RNAi plates on day 3, followed by imaging of the coelomocytes within the tail region on day 4. GFP intensity was recorded and quantified using ImageJ.

Acknowledgment

We thank the Caenorhabditis Genetic Center and Shohei Mitani of the National BioResource Project for providing strains. We thank Dr. Daniel Garsin from University of Texas Health Science Center at

Houston for sharing RNAi clones and other reagents. We thank Jina Park, an English major Rice University student, for proofreading the manuscript.

This research was supported by the University of Texas Health Science Center at Houston (37516-12002), the Rising STARs program of UT systems (26532), and National Institutes of Health (NIH) K01 (NHLBI K01HL143111).

Fluorescence microscopy was performed at the Nikon Center of Excellence - Center for Advanced Microscopy, Department of Integrative Biology & Pharmacology at McGovern Medical School, UTHealth Houston.

The authors declare no competing financial interests.

Author contributions: H-E Kim conceived the study. LA Tavizon performed ER secretion experiments and genetic crosses. R Hong performed paralysis and motility assays. TI Moore analyzed the confocal images. RG Tharyan performed worm sorter experiments. JJ Li and N Xin carried out the rest of the experiments with the help of C Yang, and analyzed the data with input from H-E Kim. JJ Li and H-E Kim took the lead in writing the manuscript. All authors discussed the results and contributed to the final manuscript. H-E Kim was in charge of the overall direction. A Antebi supervised the project performed at the Max Planck Institute for Biology of Ageing, Cologne, Germany.

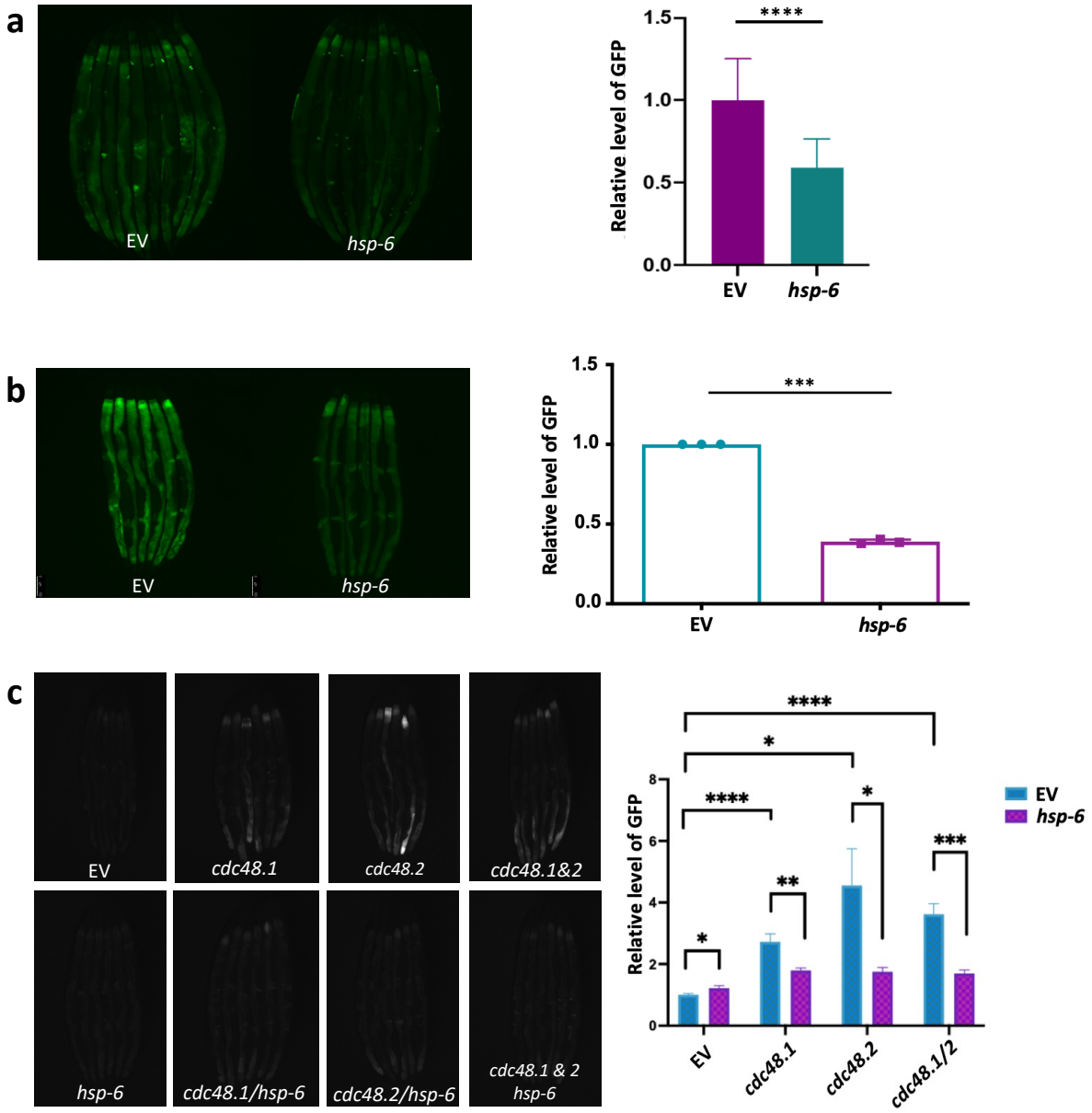
a
EV
hsp-6
****
Relative level of GFP
1.5
1.0
0.5
0.0
EV
hsp-6
b
EV
hsp-6
***
Relative level of GFP
1.5
1.0
0.5
0.0
EV
hsp-6
c
EV
cdc48.1
cdc48.2
cdc48.1&2
hsp-6
cdc48.1/hsp-6
cdc48.2/hsp-6
cdc48.1 & 2
hsp-6
****
*
****
*
**
*
***
Relative level of GFP
8
6
4
2
0
EV
hsp-6
EV
cdc48.1
cdc48.2
cdc48.1/2

Figure 1. **Inhibition of *hsp-6* results in the reduction of ER stress response.** SJ4005 (*hsp-4p*::GFP) reporter worms were grown on OP50 plates until day 1 adulthood. On day 1 of adulthood, the worms were treated with **a)** tunicamycin (TM) for 4 hours in order to induce ER stress. Following TM treatment, the worms were transferred onto RNAi-containing plates and grown at 20°C until day 4 of adulthood and were imaged to assess ER stress levels. Other forms of ER stress, including **b)** *vcp* knockdown and **c)** *nfyb-1 (cu13)* mutants knockdown was tested in the same manner to further validate that our observation was not TM specific but rather a conserved physiological mechanism. The graph shows the mean+/-SD of three biological repeats, n>=6 in each repeat.

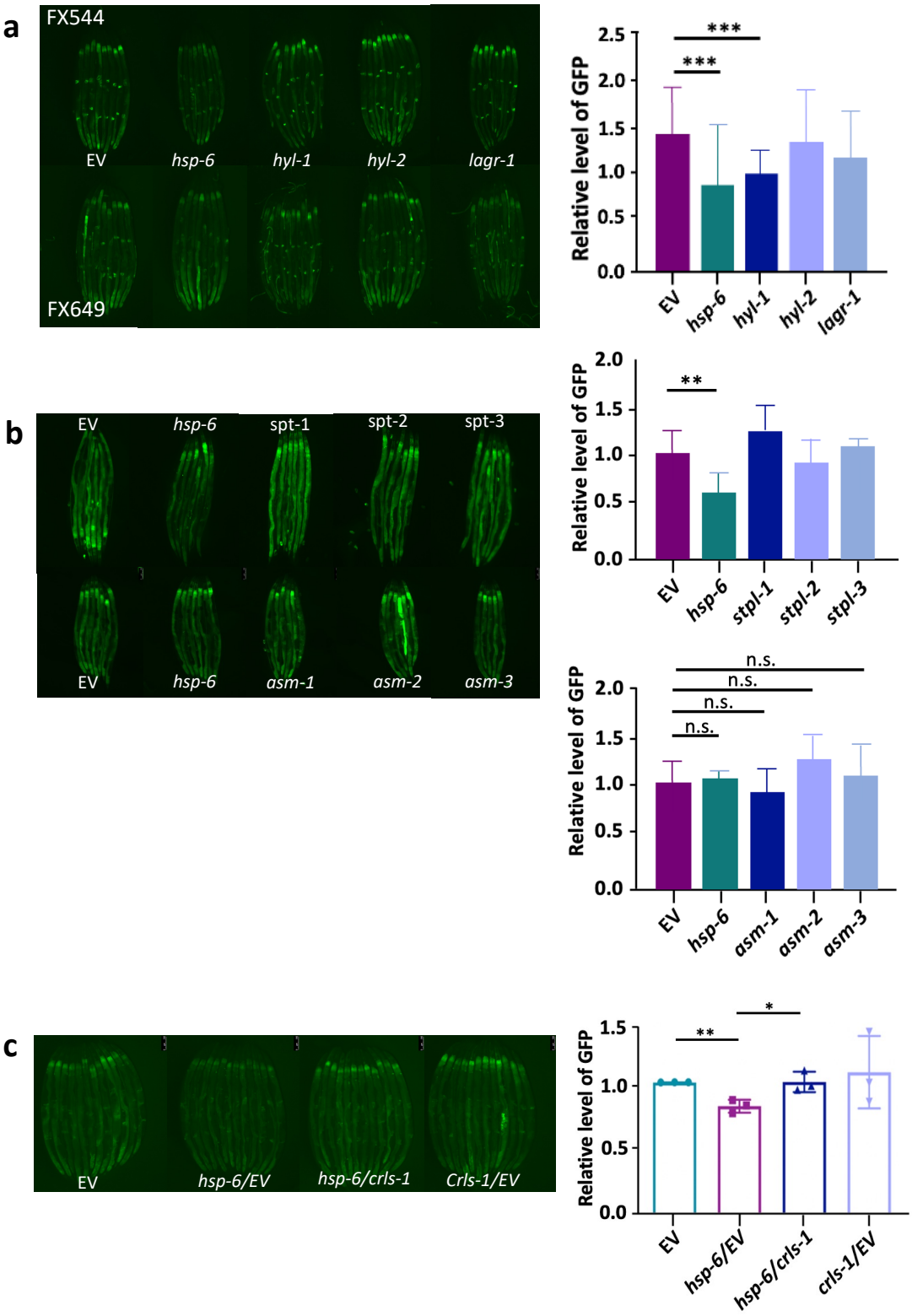
a
FX544
EV
hsp-6
hyl-1
hyl-2
lagr-1
FX649
Relative level of GFP
***
***
EV
hsp-6
hyl-1
hyl-2
lagr-1
b
EV
hsp-6
spt-1
spt-2
spt-3
EV
hsp-6
asm-1
asm-2
asm-3
Relative level of GFP
**
EV
hsp-6
stpl-1
stpl-2
stpl-3
Relative level of GFP
n.s.
n.s.
n.s.
n.s.
EV
hsp-6
asm-1
asm-2
asm-3
c
EV
hsp-6/EV
hsp-6/crls-1
Crls-1/EV
Relative level of GFP
**
*
EV
hsp-6/EV
hsp-6/crls-1
crls-1/EV

Figure 2. **The reduction of ER stress by *hsp-6* RNAi is partially regulated through lipid metabolism**. **a)** Two separate worm lines were used to determine the effects of *hyl-1*, *hyl-2* and *lagr-1* on MERSR, FX544 (*cdc48.1* knockout) and FX649 (*cdc48.2* knockout). Worms were grown to day 1 adulthood on OP50 plates, followed by a 4 hour treatment with TM for ER stress induction. Worms were transferred onto RNAi plates targeting *hyl-1*, *hyl-2* or *lagr-1* post TM treatment and incubated at 20°C till day 4 of adulthood. Worms were then imaged, and GFP fluorescence was quantified for data analysis. **b)** Other sphingolipid enzymes along the *de novo* synthesis pathway and the salvage pathways were also tested in the same manner. **c)** Knockdown of cardiolipin synthetase *crls-1* positively regulated induction of UPR^{ER}. SJ4005 animals were bleach synchronized and grown on OP50 NGM plates until late L4, when the animals were treated with 25ug/ml tunicamycin for 4 hours at 20°C. Animals were then collected and transferred to RNAi plates or the empty vector control plates. The intensity of GFP was measured 72 hours post-tunicamycin treatment. a-c: representative images of animals grown on different RNAi following tunicamycin treatment. All Fluorescence intensity was quantified with ImageJ. The graph shows the mean+/-SD of three biological repeats, n>=6 in each repeat.

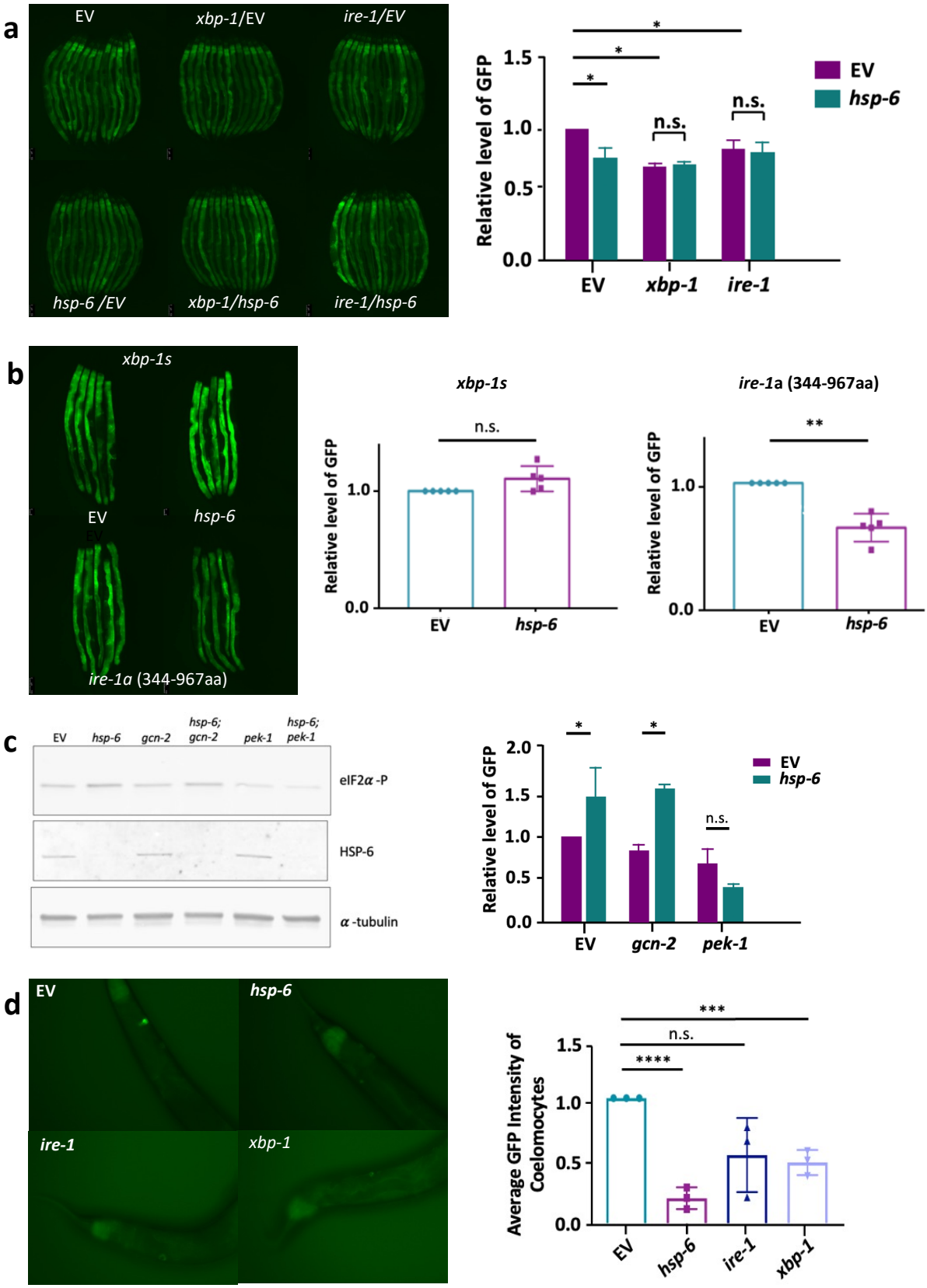
a
EV
xbp-1/EV
ire-1/EV
hsp-6 /EV
xbp-1/hsp-6
ire-1/hsp-6
Relative level of GFP
1.5
1.0
0.5
0.0
*
*
*
n.s.
n.s.
EV
hsp-6
EV
xbp-1
ire-1
b
xbp-1s
EV
hsp-6
ire-1a (344-967aa)
xbp-1s
n.s.
Relative level of GFP
1.0
0.0
EV
hsp-6
ire-1a (344-967aa)
**
Relative level of GFP
1.0
0.0
EV
hsp-6
c
EV
hsp-6
gcn-2
hsp-6; gcn-2
pek-1
hsp-6; pek-1
eIF2α -P
HSP-6
α -tubulin
Relative level of GFP
2.0
1.5
1.0
0.5
0.0
*
*
n.s.
EV
hsp-6
EV
gcn-2
pek-1
d
EV
hsp-6
ire-1
xbp-1
Average GFP Intensity of Coelomocytes
1.5
1.0
0.5
0.0
***
n.s.
****
EV
hsp-6
ire-1
xbp-1

Figure 3. **The reduction of ER stress by *hsp-6* RNAi is the result of increased ER UPR activity. a)** SJ4005 animals were bleach synchronized and grown on OP50 NGM plates until late L4, when the animals were treated with 25ug/ml tunicamycin for 4 hours at 20°C. Animals were then collected and transferred to RNAi plates or empty vector control plates. The intensity of GFP was measured 4 days post tunicamycin treatment. The graph shows 2 biological repeats with n>=8 in each repeat. **b)** MCSR regulates UPR^{ER} at the membrane level. Animals were grown on OP50 until late L4/young adult stage, then collected, washed and transferred to *hsp-6* RNAi plate or the empty vector control plate. Worms were imaged on day 3 (72 hours of RNAi treatment). *hsp-4*p::GFP*; vha-6*p::*xbp-1s* animals, *hsp-4*p::GFP*; vha-6*p::ERss::ire-1a (344-967aa) animals. The graph shows mean+/-SD of three biological repeats, n>=6 in each repeat. **c)** N2 animals were treated with EV, *gcn-2* or *pek-1* RNAi from hatch to late L4 stage, when animals were collected, washed and transferred to either fresh single RNAi plates to continue single RNAi treatment, or to *hsp-6* RNAi, *gcn-2*, *hsp-6* double RNAi, or *pek-1*, *hsp-6* double RNAi, respectively, to initiate the *hsp-6* RNAi treatment. Animals were lysed in PBS buffer with 0.1% Triton X-100. After clearing the debri, total protein level was quantified with BCA. **d)** DAF-28::GFP transgenic animals were synchronized and treated with hsp-6 RNAi, *xbp-1* RNAi, *ire-1* RNAi, or the empty vector control from day 1 of adulthood. Animals were imaged for coelomocyte GFP content on day 4. The graph shows mean+/-SD of GFP intensity normalized to empty vector control from three biological repeats, n>=5 in each repeat.

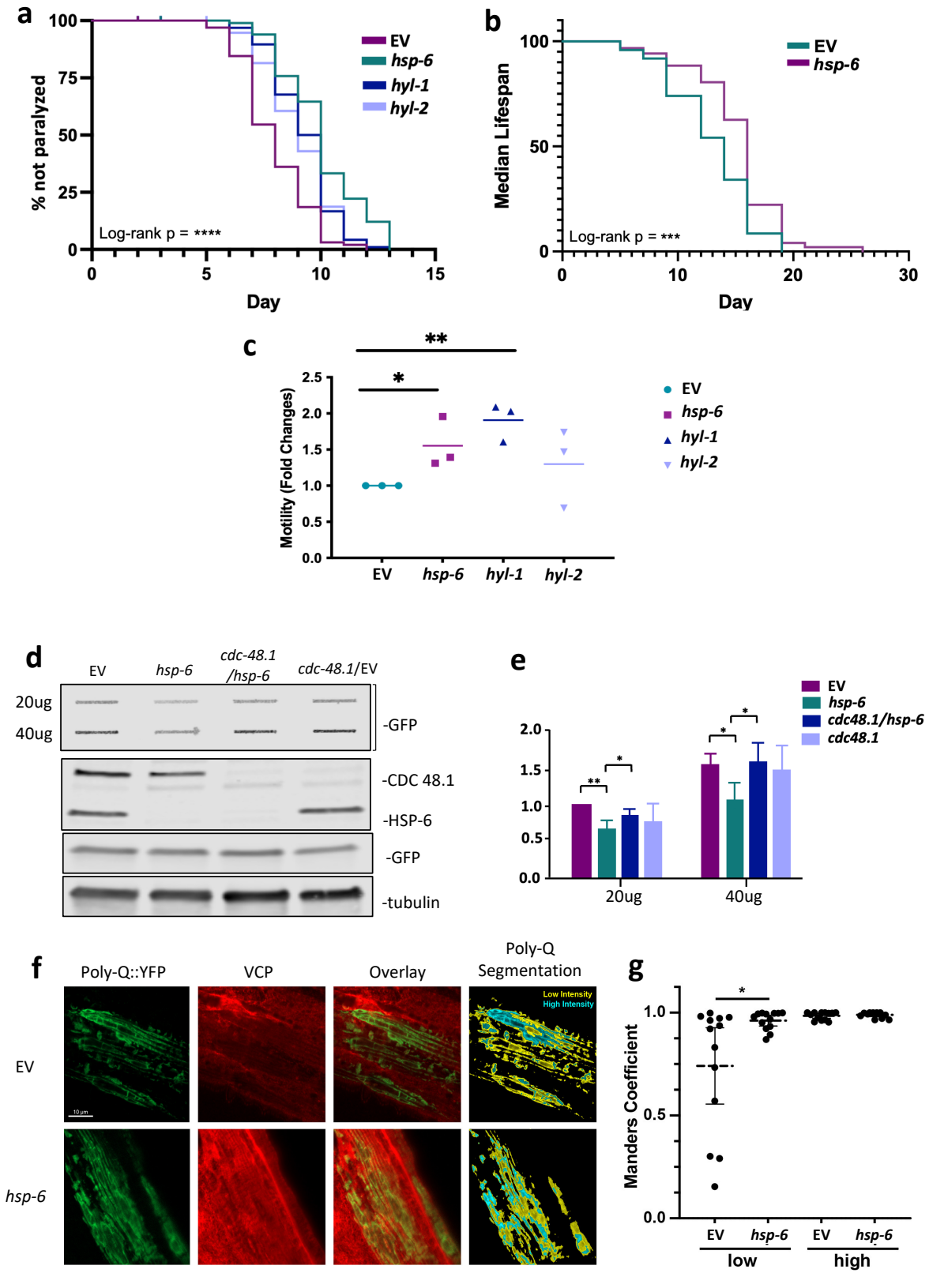
a
% not paralyzed
Day
EV
hsp-6
hyl-1
hyl-2
Log-rank p = ****
b
Median Lifespan
Day
EV
hsp-6
Log-rank p = ***
c
Motility (Fold Changes)
EV
hsp-6
hyl-1
hyl-2
d
EV
hsp-6
cdc-48.1 /hsp-6
cdc-48.1/EV
20ug
40ug
-GFP
-CDC 48.1
-HSP-6
-GFP
-tubulin
e
EV
hsp-6
cdc48.1/hsp-6
cdc48.1
20ug
40ug
f
Poly-Q::YFP
VCP
Overlay
Poly-Q Segmentation
Low Intensity
High Intensity
EV
hsp-6
g
Manders Coefficient
EV
hsp-6
EV
hsp-6
low
high

Figure 4. **The knockdown of *hsp-6* reduces protein aggregation in poly-glutamine disease model worms**. **a)** Paralysis of pan-neuronal Abeta expressing worms crossed with neuronal RNAi sensitive line (GRU102:TU3401). 100 animals per RNAi condition were incubated at 25°C during their lifespan. This mild heat shock accelerates the production of the neuronal toxic aggregates which led to paralysis. Treatment of RNAi against *hsp-6, hyl-1, hyl-2 and* EV were used to determine improvements on paralysis during heat shock. **b)** Lifespan of GRU102:TU3401 animals during the treatment of *hyl-1 and* EV. 100 animals per condition was grown at 20°C and counted daily to determine survivability. **c)** Animals expressing poly-Q aggregates (Q40::YFP) within the neurons (AM101) were crossed with a neuronal RNAi-sensitive worm line (TU3401). The resulting AM101:TU3401 showed decreased motility as the result of increased poly-Q aggregate formation within the neurons. RNAi targeting *hsp-6, hyl-1, hyl-2* and EV were given to the worms and motility was determined using a body bending assay. Worms were dropped into solution, and the number of body bends per 30 seconds was recorded and counted to determine the impact of RNAi on motility. **d)** The accumulation of poly-glutamine aggregates is reduced upon MERSR. Transgenic worms expressing poly-Q aggregates (Q35::YFP) in the body wall muscle (AM140) were treated with *hsp-6* RNAi, *cdc48.1* RNAi, double RNAi or the empty vector control from day 1 adulthood. Animals were collected on day 5. Protein aggregates were measured by applying protein lysate onto cellulose acetate membrane through a vacuum slot blotter. The membrane was blotted with GFP antibody to detect the Q35::YFP aggregates. RNAi knockdown of *hsp-6* results in less accumulation of Q35::YFP trapped on the membrane. This down regulation depends on the normal level of VCP. Additional knockdown of *cdc-48.1* abolished the effect of *hsp-6* RNAi. 20ug of total protein lysate from each RNAi treatment was applied to SDS-PAGE followed by Western blot of alpha-tubulin, GFP, VCP, and HSP-6 antibody. Total protein and total Q35::YFP protein levels were both at equivalent levels across all specimens.

The VCP blot and HSP-6 blot showed that the RNAi knockdown of targeted protein worked efficiently. **e)** Graph shows mean+-SD of filter trapped Q35::YFP from three biological repeats. **f)** Representative confocal image of polyQ::YFP (green) and VCP (red) localization in the body wall muscle of AM140 (f-A and f-B). Scale bar = 10µm. f-C) Segmentation of polyQ::YFP by emission intensity (low, yellow; high, cyan). Colocalization of VCP with polyQ as measured by the Meanders correlation in high and low-intensity areas of polyQ control and *hsp-6* knockdown worms. Bars show mean ± 95% CI. Two-tailed Mann–Whitney tests show p=0.05 (*). N (number of images) EV = 13; *hsp-6* = 14.

References

1. Hetz, C. The unfolded protein response: controlling cell fate decisions under ER stress and beyond. *Nat. Rev. Mol. Cell Biol.* **13**, 89–102 (2012).
2. Flechsler, J., Heimerl, T., Huber, H., Rachel, R. & Berg, I. A. Functional compartmentalization and metabolic separation in a prokaryotic cell. *Proc. Natl. Acad. Sci.* **118**, e2022114118 (2021).
3. Kim, H.-E. *et al.* Lipid Biosynthesis Coordinates a Mitochondrial-to-Cytosolic Stress Response. *Cell* **166**, 1539-1552.e16 (2016).
4. Rizzuto, R. *et al.* Close Contacts with the Endoplasmic Reticulum as Determinants of Mitochondrial Ca^{2+} Responses. *Science* **280**, 1763–1766 (1998).
5. Sassano, M. L., Felipe-Abrio, B. & Agostinis, P. ER-mitochondria contact sites; a multifaceted factory for Ca2+ signaling and lipid transport. *Front. Cell Dev. Biol.* **10**, 988014 (2022).
6. Yeo, H. K. *et al.* Phospholipid transfer function of PTPIP51 at mitochondria-associated ER membranes. *EMBO Rep.* **22**, e51323 (2021).
7. Friedman, J. R. *et al.* ER Tubules Mark Sites of Mitochondrial Division. *Science* **334**, 358–362 (2011).
8. Bravo, R. *et al.* Increased ER–mitochondrial coupling promotes mitochondrial respiration and bioenergetics during early phases of ER stress. *J. Cell Sci.* **124**, 2511–2511 (2011).
9. Lim, D. *et al.* Ca2+ handling at the mitochondria-ER contact sites in neurodegeneration. *Cell Calcium* **98**, 102453 (2021).

10. Simoes, I. C. M. *et al.* The mystery of mitochondria-ER contact sites in physiology and pathology: A cancer perspective. *Biochim. Biophys. Acta BBA - Mol. Basis Dis.* **1866**, 165834 (2020).
11. Wang, Y. *et al.* Endoplasmic Reticulum-Mitochondria Contacts: A Potential Therapy Target for Cardiovascular Remodeling-Associated Diseases. *Front. Cell Dev. Biol.* **9**, 774989 (2021).
12. Adams, C. J., Kopp, M. C., Larburu, N., Nowak, P. R. & Ali, M. M. U. Structure and Molecular Mechanism of ER Stress Signaling by the Unfolded Protein Response Signal Activator IRE1. *Front. Mol. Biosci.* **6**, 11 (2019).
13. Chu, Q. *et al.* Regulation of the ER stress response by a mitochondrial microprotein. *Nat. Commun.* **10**, 4883 (2019).
14. Baker, B. M., Nargund, A. M., Sun, T. & Haynes, C. M. Protective Coupling of Mitochondrial Function and Protein Synthesis via the eIF2α Kinase GCN-2. *PLoS Genet.* **8**, e1002760 (2012).
15. Anderson, N. & Haynes, C. M. Folding the Mitochondrial UPR into the Integrated Stress Response. *Trends Cell Biol.* **30**, 428–439 (2020).
16. Xiao, T. *et al.* Mitochondrial stress protein HSP60 regulates ER stress-induced hepatic lipogenesis. *J. Mol. Endocrinol.* **64**, 67–75 (2020).
17. Ahlstedt, B. A., Ganji, R. & Raman, M. The functional importance of VCP to maintaining cellular protein homeostasis. *Biochem. Soc. Trans.* **50**, 1457–1469 (2022).

18. Szczęśniak, P. P., Heidelberger, J. B., Serve, H., Beli, P. & Wagner, S. A. VCP inhibition induces an unfolded protein response and apoptosis in human acute myeloid leukemia cells. *PLOS ONE* **17**, e0266478 (2022).
19. Tharyan, R. G. *et al.* NFYB-1 regulates mitochondrial function and longevity via lysosomal prosaposin. *Nat. Metab.* **2**, 387–396 (2020).
20. Mosbech, M.-B. *et al.* Functional Loss of Two Ceramide Synthases Elicits Autophagy-Dependent Lifespan Extension in C. elegans. *PLoS ONE* **8**, e70087 (2013).
21. Hwang, J., Peterson, B. G., Knupp, J. & Baldridge, R. D. The ERAD system is restricted by elevated ceramides. *Sci. Adv.* **9**, eadd8579 (2023).
22. Wang, H. *et al.* The Endoplasmic Reticulum Chaperone GRP170: From Immunobiology to Cancer Therapeutics. *Front. Oncol.* **4**, (2015).
23. Wek, R. C. Role of eIF2α Kinases in Translational Control and Adaptation to Cellular Stress. *Cold Spring Harb. Perspect. Biol.* **10**, a032870 (2018).
24. Garcia, G. *et al.* Lipid homeostasis is essential for a maximal ER stress response. *eLife* **12**, e83884 (2023).
25. Ganji, R. *et al.* The p97-UBXD8 complex regulates ER-Mitochondria contact sites by altering membrane lipid saturation and composition. *Nat. Commun.* **14**, 638 (2023).
26. Hou, N. S. *et al.* Activation of the endoplasmic reticulum unfolded protein response by lipid disequilibrium without disturbed proteostasis in vivo. *Proc. Natl. Acad. Sci.* **111**, (2014).
27. Walter, P. & Ron, D. The Unfolded Protein Response: From Stress Pathway to Homeostatic Regulation. *Science* **334**, 1081–1086 (2011).

28. Wek, S. A., Zhu, S. & Wek, R. C. The Histidyl-tRNA Synthetase-Related Sequence in the eIF-2␣ Protein Kinase GCN2 Interacts with tRNA and Is Required for Activation in Response to Starvation for Different Amino Acids. *MOL CELL BIOL* **15**, (1995).
29. Pierce, S. B. *et al.* Regulation of DAF-2 receptor signaling by human insulin and *ins-1* , a member of the unusually large and diverse *C. elegans* insulin gene family. *Genes Dev.* **15**, 672–686 (2001).
30. Li, W., Kennedy, S. G. & Ruvkun, G. *daf-28* encodes a *C. elegans* insulin superfamily member that is regulated by environmental cues and acts in the DAF-2 signaling pathway. *Genes Dev.* **17**, 844–858 (2003).
31. Fares, H. & Greenwald, I. Genetic Analysis of Endocytosis in *Caenorhabditis elegans* : Coelomocyte Uptake Defective Mutants. *Genetics* **159**, 133–145 (2001).
32. Safra, M. & Henis-Korenblit, S. A new tool in *C. elegans* reveals changes in secretory protein metabolism in *ire-1* -deficient animals. *Worm* **3**, e27733 (2014).
33. Lindholm, D., Wootz, H. & Korhonen, L. ER stress and neurodegenerative diseases. *Cell Death Differ.* **13**, 385–392 (2006).
34. Katayama, T. *et al.* Presenilin-1 mutations downregulate the signalling pathway of the unfolded-protein response. *Nat. Cell Biol.* **1**, 479–485 (1999).
35. Hetz, C. & Saxena, S. ER stress and the unfolded protein response in neurodegeneration. *Nat. Rev. Neurol.* **13**, 477–491 (2017).
36. Lee, D. Y. *et al.* Activation of PERK Signaling Attenuates Aβ-Mediated ER Stress. *PLoS ONE* **5**, e10489 (2010).

37. Haass, C., Koo, E. H., Mellon, A. & Hung, A. Y. p-amyloid precursor protein to. **357**, (1992).

38. D'Silva, P., Liu, Q., Walter, W. & Craig, E. A. Regulated interactions of mtHsp70 with Tim44 at the translocon in the mitochondrial inner membrane. *Nat. Struct. Mol. Biol.* **11**, 1084–1091 (2004).

39. Xu, L., Voloboueva, L. A., Ouyang, Y. & Giffard, R. G. Overexpression of Mitochondrial Hsp70/Hsp75 in Rat Brain Protects Mitochondria, Reduces Oxidative Stress, and Protects from Focal Ischemia. *J. Cereb. Blood Flow Metab.* **29**, 365–374 (2009).

40. Qu, M. *et al.* Mortalin overexpression attenuates beta-amyloid-induced neurotoxicity in SH-SY5Y cells. *Brain Res.* **1368**, 336–345 (2011).

41. Liu, F. *et al.* Involvement of mortalin/GRP75/mthsp70 in the mitochondrial impairments induced by A53T mutant α-synuclein. *Brain Res.* **1604**, 52–61 (2015).

42. Priyanka & Seth, P. Insights Into the Role of Mortalin in Alzheimer's Disease, Parkinson's Disease, and HIV-1-Associated Neurocognitive Disorders. *Front. Cell Dev. Biol.* **10**, 903031 (2022).

43. Honrath, B. *et al.* Glucose-regulated protein 75 determines ER–mitochondrial coupling and sensitivity to oxidative stress in neuronal cells. *Cell Death Discov.* **3**, 17076 (2017).

44. Wadhwa, R. *et al.* Inactivation of Tumor Suppressor p53 by Mot-2, a hsp70 Family Member. *J. Biol. Chem.* **273**, 29586–29591 (1998).

45. Lu, W.-J. *et al.* Mortalin–p53 interaction in cancer cells is stress dependent and constitutes a selective target for cancer therapy. *Cell Death Differ.* **18**, 1046–1056 (2011).
46. Schlame, M. & Greenberg, M. L. Biosynthesis, remodeling and turnover of mitochondrial cardiolipin. *Biochim. Biophys. Acta BBA - Mol. Cell Biol. Lipids* **1862**, 3–7 (2017).
47. Gebert, N. *et al.* Mitochondrial Cardiolipin Involved in Outer-Membrane Protein Biogenesis: Implications for Barth Syndrome. *Curr. Biol.* **19**, 2133–2139 (2009).
48. Fiedorczuk, K. *et al.* Atomic structure of the entire mammalian mitochondrial complex I. *Nature* **538**, 406–410 (2016).
49. Dores-Silva, P. R., Cauvi, D. M., Kiraly, V. T. R., Borges, J. C. & De Maio, A. Human HSPA9 (mtHsp70, mortalin) interacts with lipid bilayers containing cardiolipin, a major component of the inner mitochondrial membrane. *Biochim. Biophys. Acta BBA - Biomembr.* **1862**, 183436 (2020).
50. Chu, C. T. *et al.* Cardiolipin externalization to the outer mitochondrial membrane acts as an elimination signal for mitophagy in neuronal cells. *Nat. Cell Biol.* **15**, 1197–1205 (2013).
51. Kagan, V. E. *et al.* Cytochrome c acts as a cardiolipin oxygenase required for release of proapoptotic factors. *Nat. Chem. Biol.* **1**, 223–232 (2005).
52. Zhong, X. *et al.* AAA ATPase p97/Valosin-containing Protein Interacts with gp78, a Ubiquitin Ligase for Endoplasmic Reticulum-associated Degradation. *J. Biol. Chem.* **279**, 45676–45684 (2004).

53. Kobayashi, T., Manno, A. & Kakizuka, A. Involvement of valosin-containing protein (VCP)/p97 in the formation and clearance of abnormal protein aggregates. *Genes Cells* **12**, 889–901 (2007).
54. Van Den Boom, J. & Meyer, H. VCP/p97-Mediated Unfolding as a Principle in Protein Homeostasis and Signaling. *Mol. Cell* **69**, 182–194 (2018).
55. Hill, S. M. *et al.* VCP/p97 regulates Beclin-1-dependent autophagy initiation. *Nat. Chem. Biol.* **17**, 448–455 (2021).
56. Chen, J., Bassot, A., Giuliani, F. & Simmen, T. Amyotrophic Lateral Sclerosis (ALS): Stressed by Dysfunctional Mitochondria-Endoplasmic Reticulum Contacts (MERCs). *Cells* **10**, 1789 (2021).
57. Du, Y., Wang, J., Xiong, J., Fang, N. & Ji, W.-K. VPS13D interacts with VCP/p97 and negatively regulates endoplasmic reticulum–mitochondria interactions. *Mol. Biol. Cell* **32**, 1474–1486 (2021).
58. Stiernagle, T. Maintenance of C. elegans. *WormBook* 1–11 (2006).
59. Kamath, R. S. *et al.* Systematic functional analysis of the Caenorhabditis elegans genome using RNAi. *Nature* **421**, 231–237 (2003).
60. Porta-de-la-Riva, M., Fontrodona, L., Villanueva, A. & Cerón, J. Basic Caenorhabditis elegans Methods: Synchronization and Observation. *J. Vis. Exp.* 4019 (2012) doi:10.3791/4019.